Reduction kinetics and mass transport of ZnO single entities on a Hg ultramicroelectrode (UME)

Nelum Karunathilake,(1) Salvador Gutierrez-Portocarrero,(1) Pradeep Subedi and Mario A. Alpuche-Aviles*

(1) These authors contributed equally to this work

Department of Chemistry, University of Nevada, Reno, Nevada 89557

Abstract

We discuss the electrolysis mechanism of colloidal ZnO NPs (10 nm diam.) in CH_3CN. Stripping the preconcentrated Zn(Hg) allows quantification of the ZnO electrolyzed during stochastic interactions with the Hg surface. We model the mass transport taking the charged agglomerates of ZnO NPs as ionic species to calculate their migration and diffusional contributions. In unsupported suspensions, the mobility and positive zeta potential enhance transport towards the Hg UME. The NP electrolysis generates ionic species, increasing the migration rate and allowing lower detection limits compared to weakly supported suspensions, where the electrolyte modifies agglomerate charge and colloidal properties. We determine the kinetic constant ($k_{f,}$ in cm/s) for the ZnO reduction from the electrolysis transient model for destructive collisions of single entities, corrected for the potentiostat time constant. While most reduction events happen within 100 ms, the single entity model is consistent with mass transport studies over longer experimental times (1800 s).

1. Introduction

We present a mechanistic study of the reduction of ZnO NPs suspended on a Hg UME. The time scale of the experiments goes from diffusion or migration limited at minutes or longer, while at short intervals (< 1s), we resolve the details of single entities colliding with the Hg surface. At short intervals, the kinetics of ZnO reduction limit the overall reduction rate and we determine the rate constant of electron transfer. At longer time scales, migration enhances the collision rate significantly in the detection of ZnO nanoparticles, with the larger enhancement without the use of supporting electrolyte. We discuss how the normally considered inert electrolyte plays a role in the agglomeration of metal oxide suspensions, on how in turn, agglomeration can change the shape of the concentration dependence. Since the seminal work by Lemay[1] and Bard,[2] single entity electrochemical measurements is now an active area of research that includes investigating reactions at metal nanoparticle.[3] The work on nanoimpacts,[4] catalysis,[5] electrocatalysis,[2b] is motivated by the need to understand the particle by particle contribution towards the reactivity of nanomaterials. We note that there are relatively few examples in the literature for discrete electrochemistry of metal oxides and semiconductors. Our group has been interested in studying the photoelectrochemistry of colloidal TiO_2,[6] sensitized TiO_2 [7] and other groups have studied photoelectron injection from single entities.[8] We propose that ZnO electrochemistry at the nanometer scale[9] is a model for metal oxides and other semiconducting materials used in energy conversion and storage. For example, we are interested in expanding the ZnO reduction to studies in aqueous systems related to Zn/air batteries (e.g., ref [10]).

Electrochemical studies of colloidal metal oxides have broad applications. Initial reports consisted of ensemble measurements of particles colliding with an electrode.[11] These included

incorporating particles from a colloidal suspension onto a metal deposit (composite materials).[12] Bard,[13][1] Kamat[14] and Grätzel[15][2] used colloidal suspensions (slurries) to investigate the photoelectrochemistry of particulate semiconductors., Heyrovsky et al. studied the polarography and voltammetry of aqueous SnO_2,[16] TiO_2,[17] and TiO_2 colloids mixed with Fe^{3+} precursors.[18] The electrochemistry of colloidal Fe_2O_3 was also the object of investigations.[19] Besides Fe_2O_3, studies in the nanoscale include the electrochemical transformation of Ag to Ag_2O and silver halides.[20] The electrodeposition of Ge nanowires from dissolved GeOx is another example of the direct oxide reduction.[21] However, in these earlier papers, the study focused on average properties and our interest is in the electrochemistry of discrete NPs. Here we study the mass transport and reduction kinetics of single entities that consist of agglomerates of ZnO. We collected information on the transients observed in these conditions and we fit the transients to a recently proposed model.[22] We investigated the effect of the potentiostat time constant[23] given the time scale of our measurements, and we propose a method to compensate for the potentiostat response. To the best of our knowledge, we present the first example for measuring a kinetic rate constant based on the direct nanostructure electrolysis under conditions limited by electron transfer kinetics. Besides the elegant determination of the rate constant for Ag oxidation from the random walk model,[24] based on a single NP getting sequentially oxidized during multiple collisions, we are not aware of additional rate constant measurements from electrolysis of nanostructures.

The kinetic model provides measurements of agglomerate size that are consistent with our transport modeling of colloidal ZnO, once we account for the effect of migration. Migration is important in single entity measurements on colloidal suspensions, in contrast to experiments in solutions that are usually limited by diffusion.[1, 25] The effect of migration in NP detection has been the object of study[26] and applications that rely on migration have been developed, including the ultra-sensitive analysis of solution,[26a] the imaging of NPs[26e, 26k][3] and positioning NPs on a substrate for the electrochemical study or catalytic[26c] properties. Here, we demonstrate that the mass transport of unsupported solutions favors the detection of ZnO NPs. We study the effect of migration in the stochastic detection of ZnO NPs of ca. 10 nm in diameter, and the interactions of the NPs with the electrolyte complicates the expected effect of a low concentration (1 mM) of salt.

Theoretical Model

We consider two stages of the ZnO nano-impact experiments. First, the mass transport of a particle on the surface of the UME. Second, the electrochemical transient recorded as evidence of the collision and reduction of ZnO to Zn(Hg). In this study, the potential applied is enough for the reduction of the zinc from the metal oxide phase, ZnO, to the amalgam-forming deposition step according to:

$$\mathrm{Zn}^{II}(\mathrm{ZnO}) + 2\mathrm{e} \rightarrow \mathrm{Zn(Hg)} \qquad (1)$$

We study the reduction of the ZnO NP in a non-aqueous system, acetonitrile because the potentials needed to reduce the NPs (−2.4 V vs Ag/AgCl(KCl=1M)) are negative of the standard aqueous system. In these experiments, we reduce Zn^{2+} on a Hg electrode to form the well-known Zn(Hg) amalgam. The standard potential of reaction is −0.956 V vs. Ag/AgCl in an aqueous system:[27]

$$\mathrm{Zn}^{2+} + 2\mathrm{e} \rightarrow \mathrm{Zn(Hg)} \qquad (2)$$

Thus, the potential applied in the preconcentration step to reduce the Zn^{2+} in ZnO is significantly more negative than the Zn(Hg) amalgam formal potential, because ZnO is harder to reduce than Zn^{2+}:

$$\mathrm{ZnO} + 2\mathrm{e} \quad \rightarrow \mathrm{Zn(Hg)} + O^{2-} \rightarrow \mathrm{Zn(Hg)} + Y^{n-} \qquad (3)$$

Where Y^{-} denotes a byproduct of the reduction of ZnO with a negative charge to account for the negative charge in the oxide ion. Here we apply models to determine the rates of reaction (3) to gain insight into the electrochemical process at the nanometer scale.

1.1 Electrolysis in Stochastic Collisions

We model the ZnO mass transport to predict the expected amount of Zinc reduced. We assume that every collision results in the reduction of ZnO entities as in eq. (2). The collision frequency, f_p, will be given by the total flux, j_T, times the electrode area, A:

$$f_P = j_T \cdot A \qquad (4)$$

For a hemispherical Hg UME, eq (4) becomes (5) because of the hemispherical diffusional flux:

$$f_{P,D} = 2\pi D_{NP} C^*_{NP} r_{WE} \qquad (5)$$

Assuming that every collision results in the electrolysis of the ZnO NP and its agglomerates, the total charge recovered in the anodic stripping voltammetry will be given by the product of the frequency of collisions, $f_{P,D}$, times the number of mol of electrons per NP, n_{NP}:

$$Q = i_{ss} t = n_{NP} F f_{P,D} t = n_{NP} F t (2\pi D_{NP} C^*_{NP} r_{WE}) \qquad (6)$$

Where i_{ss} is the steady-state current, D_{NP} is the particle diffusion coefficient, C^*_{NP} is the NP bulk concentration and r_{WE} is the radius of the Hg hemisphere electrode, t is the time, F is Faraday's constant. We demonstrate that the stripping of Zn can be quantitatively accounted for when migration is considered. For ionic solutions, the steady-state current increases in unsupported systems because the migration contribution becomes significant with respect to the diffusion rate. Oldham[28] and Amatore[29] studied the effect of migration on UMEs on weakly supported solutions.[30] Here we use the expression of Amatore[29] as used by White et al.[31] For the simplest case, the steady-state current (i_{ss}) of an unsupported solution will increase the diffusion current (i_D) by a factor k_m. When n = z, eq. (7),

$$i_{ss}/i_D = k_m = 1 + |n| \qquad (7)$$

For every other case, eq. (8) applies:

$$i_T/i_D = k_m = 1 \pm z\left\{1 + (1 + |z|)(1 - z/n) \cdot ln\left(1 - \frac{1}{[(1+|z|)(1-z/n)]}\right)\right\} \qquad (8)$$

where the sign in eq. (8) is negative for n > z and positive for n < z. Thus, by multiplying the expected diffusional current by the factor k_m we can calculate the expected total current, accounting for migration.

1.2 Electrolysis Current Transients

We model charge transfer transients during nano-impact events that result in electrolysis of single entities. We address the electrolysis of individual ZnO agglomerates at the Hg interface using a model first proposed for the electrolysis of Ag NPs. [22, 32] First, the model implies entity/electrode contact or a distance within tunneling from the interface. Second, the reaction is irreversible; this assumption applies here because the ZnO reduction yields an amalgam at high overpotentials so metal atoms in ZnO are incorporated into the mercury working electrode. Lastly, the model assumes that the process is kinetically-limited, that is, that the kinetics of ZnO reduction limit the rate of reduction and not mass transport. We base this analysis on the shapes of the models derived by Kätelhön et al.,[22], Here, we rederived the model using different experimental constants, adapting the nomenclature used previously.[22] The limiting rate $j_{lim,kin}$ of the species being electrolyzed eq. (9) is proportional to the projected area of the particle because the entity has to be within tunneling distance of the electrode surface. [32]

$$j_{lim,kin} = k_f C_{ZnO}^{Zn} \quad (9)$$

The details of the kinetic model derivation are in the SI (section S7), and the final equation is:

$$i(t) = nF\pi \left(\frac{k_f}{V_m}\right)\left[r_0 - \frac{k_f}{4}t\right]^2 \quad (10)$$

Where r_0 is the initial radius of the NP being reduced, and V_m is the crystallographic density. We obtain the value of V_m from the crystallographic data of ZnO because (the unit cell of the in-lab synthesized NPs used in this work corresponds to zincite, see Figure S1 and S3).

2. Experimental Section

We previously reported the detailed procedure to electrolyze ZnO NPs.[33] Briefly, a Hg ultramicroelectrode (working electrode, see Supporting Information, SI, section S3), Pt wire counter electrode and a reference electrode of Ag/AgCl (KCl = 1M) inside a fritted glass double junction were used in a standard three-electrode cell configuration. All electrodes were dipped in purified CH_3CN, and Ar was bubbled through the solution for 15 minutes to purge O_2 in solution. CH_3CN was purified to remove traces of metal ions.[34] Then ZnO NPs (SI, section S2 for synthesis method) with zincite phase (SI, section S4 for characterization) were injected and purged with Ar was continued for another 5 minutes. The Hg ultramicroelectrode was inserted into the system after making an Ar blanket on top of the solution. ZnO was reduced at a fixed potential of −2.4 V vs Ag/AgCl(KCl=1M)//CH3CN// to form Zn(Hg) for 1800 s. Immediately after the collision experiment, linear sweep voltammetry was carried out in anodic direction to oxidize any reduced Zn(Hg) into Zn^{2+}, i.e., to strip cations of zinc back into the solution. In the graphs shown here, cathodic currents are positive

3. Results and Discussion

The experimental data for the reduction of the ZnO NPs of ca. 10 nm diameter at different concentrations is described in Figure 1. The current trace data for the reduction of ZnO NPs shows discrete changes as well as spikes. To determine the frequency of collisions and the stochastic models in this part of the work, we are interested in the accumulation of Zn(Hg) over long periods of time (1800 s, 32 ms sampling interval). Figure 1 also shows the control experiment for CH_3CN blank (without NPs) under the same experimental conditions. Therefore, the transients observed are the result of ZnO NPs collisions at the different concentrations of 5 nM, 10 nM, 20 nM, 40 nM, 60 nM, and 80 nM. For this experiment, the reduction was carried out at –2.4 V with respect to Ag/AgCl. Both systems where tested unsupported (Figure 1a), without supporting electrolyte, and supported (Figure 1b), with 1 mM of tetra-n-butylammonium perchlorate, TBAP.

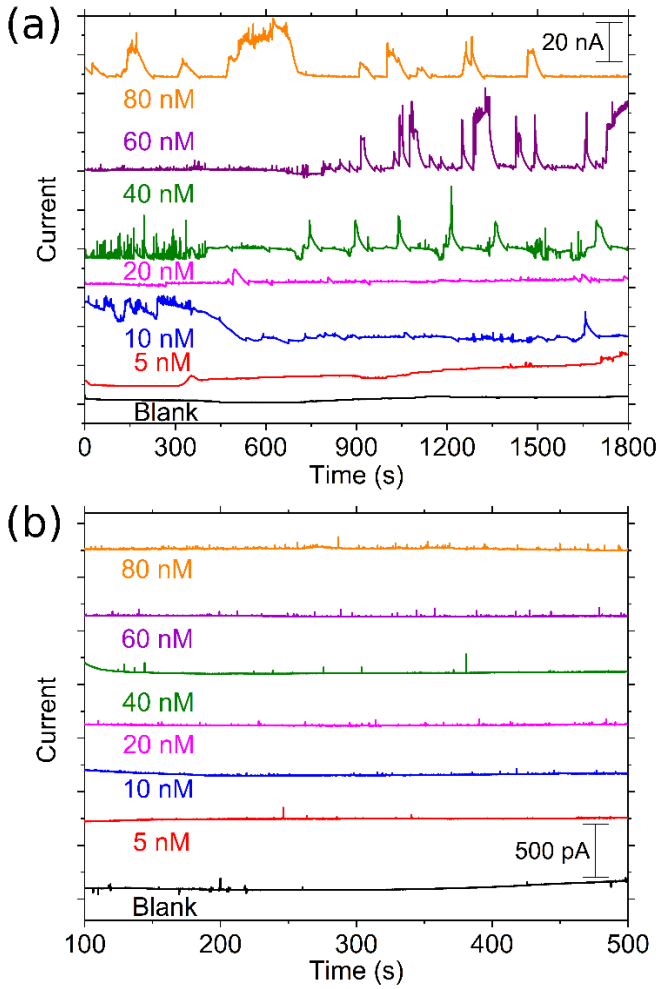

Figure 1. Current vs. time curve for the reduction of ZnO NP, ca. 10 nm in diameter at different concentrations, where the blank is acetonitrile, neat or with TBAP, for comparison. (a) Unsupported colloid, and (b) supported with 1 mM of TBAP. E_{app}= –2.4 V vs. Ag/AgCl.

The shape of the current vs. time response is used to interpret the nature of the NP interactions with the working UME. It is interesting to note that the data in Figure 1a and (b), although low resolution, display two types of phenomena, step-wise incremental response and blips or

spikes, in the current density. Previous reports assigned spikes or "blips" in the current vs. time response when the particles do not attach to the electrode surface,[35] or in the use of Hg indicating electrodes, the detection of Pt NPs under electrocatalytic amplification results in blips because the Pt dissolves into the Hg.[36] Therefore, we interpret the results in Figure 1(a) and (b) as the transient response of the reduction of ZnO, and the larger currents are the result of larger aggregates or the simultaneous reduction of several smaller single entities on the Hg surface. The currents of the cathodic spikes correspond to several thousands of ZnO NPs based on the charge it would take to reduce a single 10 nm NP (6.95×10^{-15} C, vide supra) with the response in these spikes being in the 10^{-10} C range. For the step-wise increase, we propose that are due to the change of properties of the Hg interface once partially reduced ZnO and the Zn from the reduction process accumulate at the interface because, in the short time scale experiments described in detail below, we observed spikes and not steps. Thus, in the longer-time study, the reducing interface is modified by the step-wise increments in the *i-t* transient into Zn(Hg), which is consistent with electrocatalytic reactions giving rise to the step-wise response.[2a] This result is less noticeable in the supported system (Figure 2c) because the anodic sweep voltammetry shows less amount of collisions when increasing the concentration of ZnO entities; because of the lower collision rate, and lower electrolysis events, there is less of a change on the Hg surface. Also, the low frequency of these cathodic events (Table 1) is not consistent with the amount of accumulated Zn during the reduction process in the long-time experiments (1800 s). As we will discuss below, the sampling rate of 32 ms per data point, is not fast enough to resolve all of the events because most happen within 100 ms. Therefore, the Zn^{2+} stripping gives the expected total charge from the collisions even when the instrumentation cannot resolve all the discrete reduction events. Beside instrumentation effects, the observed collision frequency could be due to other complications (agglomeration, skewed Brownian motion, colloid stability), but because of the amount of accumulated Zn correlates with the migration model it follows that the differences observed here are due to the lower sampling rate and not having enough S/N to resolve the Hg/ZnO collisions. Thus, we increased the sampling rate to improve signal resolution, and we discuss the results below. **Table 1**. Frequency of reductive transients for unsupported and supported ZnO suspensions and theoretical value of collision per second. The instrumentation sampling rate and S/N limit the number of observed collision frequencies (see text for details)

Observed reduction events observed in Figure 1		Expected
Figure 1 a) 40 nM ZnO, unsupported	Figure 1b. 40 nM ZnO with 1 mM TBAP	Based on eq. (5)
382	205	9×10^6

Figure 2(a), (b) and (e) show the detail of a 40 nM ZnO colloid *i-t* transients where the spikes while Figure 2(c) shows the stripping of Zn^{2+} during a potential scan in the positive direction. We use the Zn^{2+} redissolution peak to determine the amount of reduced ZnO. Figure 2e shows the details of the *i-t* transient. Note that these data set have lower resolution, and therefore, we provide higher resolution studies below by sampling at higher rates. In the faster sampling rates, the effect of the instrumentation delay is the main factor that limits the shape of the response. For the supported system, we did not obtain a linearly increasing calibration curve, so we focused our analysis on the unsupported system. The concentration dependence studies confirm the stripping peaks around −1.5 V are due to the oxidation of Zn(Hg). [9b] The stripping voltammogram is

obtained immediately after the preconcentration step of 40 nM ZnO colloids for a time of 1800 s. Figure 2(a) and (b) show a zoom-in of the spikes in the *i*-t transients for the unsupported and supported suspensions, respectively. The observed current for the spikes of the unsupported colloid are larger than those observed in the supported system (compare scale in Figure 2(a) and (b)). These collisions are assigned to smaller agglomerates since the large ones will precipitate based on the stability of the colloid, see SI (section S5), and Table 2 for zeta potentials.

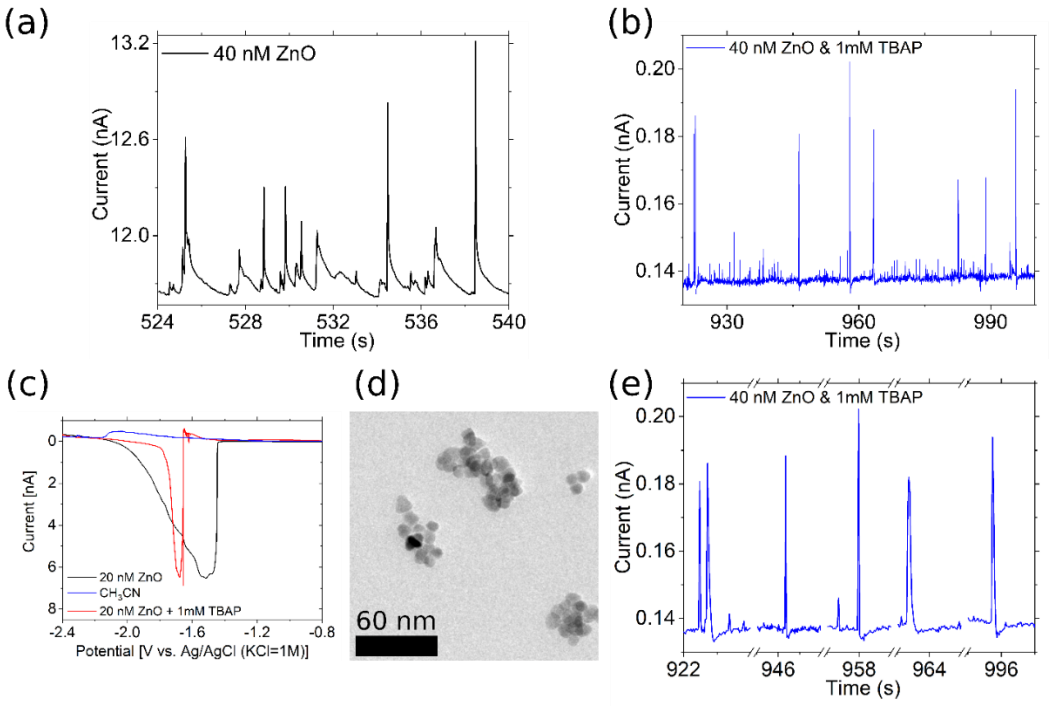

Figure 2. Current transients for a ZnO suspension at E_{app}= –2.4 V vs. Ag/AgCl. (a) Detail of the unsupported system, and (b) supported (1 mM TBAP). (c) Linear sweep voltammetry curve of the two systems (–––, black unsupported, ––– red, + 1mM TBAP) and the blank (–––, blue). (d) TEM image of ZnO entities with an average diameter of 60 nm scale. (e) Detailed *i-t* transients of the supported data in (b). Note the breaks of the *x*-scale.

Figure 3 shows the charge for the Zn^{2+} re-dissolution in the anodic scan at different concentrations of ZnO. The graph shows the results for unsupported suspensions (Figure 3a) and models of diffusion and migration. Figure 3(b) is the comparison of the supported (1 mM TBAP) and unsupported ZnO suspensions. The addition of TBAP results in a non-linear calibration curve that decreases the charge at higher concentrations and that would not be useful for analytical applications. Interestingly, the use of unsupported NPs yields a linear calibration curve. Furthermore, these results are consistent with the low frequency of collisions observed for this system (Table 1), compared to the supported system. We interpret these differences as the results of greater agglomerationthat increases with the concentration of ZnO. This is an unexpected result because solutions with small concentrations of electrolyte (e.g., 1 mM) like the one used in this work, normally stabilize colloidal systems. [37] To investigate these effects we performed DLS studies of the two NPs suspensions (see SI, section S5). Figure S4 shows the characterization by DLS for two different cases of NP suspensions, (black) without supporting electrolyte and (red) with the addition of 1 mM TBAP.

Note that this theoretical treatment in equations (7-8) assumes that the total current will be a constant factor of the diffusional component, k_m. Based on the results of Figure 3, this assumption holds for the unsupported suspension, but the addition of electrolyte changes the colloidal behavior completely. There are several assumptions built into the model. Most significantly, equations (7-8), were derived under the assumption that electroneutrality is conserved during the electrolysis, an assumption that does not hold here at low concentrations when impurities in CH_3CN and colloidal properties limit the transport of NPs by migration. The model in equation (6) yields the line in Figure 3 based on diffusion (——, yellow line) in Figure 3(a). The line is calculated based on the measurements of diffusion coefficients obtained by DLS (SI, section S5). We note that the diffusion coefficients, and therefore, the model correspond to agglomerates that are larger in diameter than the values expected for a ca. 10 nm diameter NP. Interestingly, the number of NPs/agglomerate will cancel out of equation (6) if the number of NPs per agglomerate is constant because it will divide the C^*_{NP} and multiply the n_{NP} value (details in the SI, section S6).

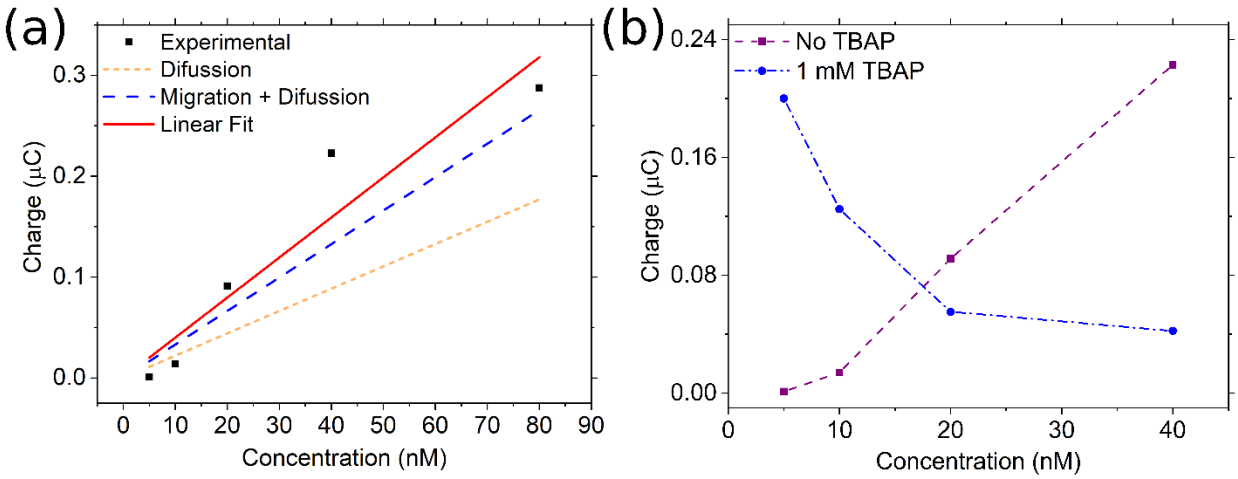

Figure 3. Charge of Zn(Hg) stripping peak as a function of ZnO NP concentration. (a) in the absence of supporting electrolyte and (b) with 1 mM TBAP. The lines in (a) show the linear regression (——, red), the experimental data (●), the expected response based on the diffusion model (——, yellow) and the migration model (——, blue). The lines in (b) show the experimental data for unsupported (——, purple) and supported 1 mM TBAP (——, blue).

We were able to observe by TEM agglomerates (Figure 2d) that agree with the 52 nm diameter entity detected by DLS. To account for the differences in mass transport, we measured the NPs zeta potential, mobility and diffusion coefficients. Table 2 summarizes the NP properties and includes transport properties for the supporting electrolyte in CH_3CN for the TBA^+ and ClO_4^- ions from ref [38]. Based on the properties in Table 2 and the data in Figure S4, we now discuss the transport properties and the expected slopes for the calibration curve of charge vs. NP concentration (see below). Figure S6 (SI) shows a calibration curve for three different ZnO batches; these different batches result in wide variabilities on the analytical signal due to the significant differences in the colloidal properties (note the error bars). Although the experiments follow the same trend, the variability is high) However, the data in this paper contains experiments conducted with the same ZnO batch yield consistent results. The migration model and the kinetic studies of ZnO electrolysis yield charges within 30% based on the DLS size applied to the migration model, and the integration of the fast reduction transient.

Table 2. Transport parameters for the colloidal suspension in this work.

Parameter	40 nM ZnO unsupported	40 nM ZnO with 1 mM TBAP	Bu_4N^+ (a)	ClO_4^- (a)
Diffusion Coefficient (D) [$cm^2\ s^{-1}$]	[5.60 ± 0.03] x10^{-8}	[1.91 ± 0.03] x 10^{-8}		
Mobility (μ) [$cm^2\ V^{-1}\ s^{-1}$]	[2.56 ± 0.03] x 10^{-4}	– [4.40 ± 0.06] x 10^{-5}	6.38 x 10^{-4}	1.073 x 10^{-3}
Zeta potential [mV]	12.7 ± 0.2	– 2.2 ± 0.3		
Absolute Charge [C]	117.41	– 59.79		

(a) Bu_4N^+ and ClO_4 data are form reference [38]

The migration behavior described above is also consistent with the data in Table 2. The zeta potential for the unsupported suspension is positive which indicates that the NPs will migrate towards the cathode. Upon addition of electrolyte, the NPs produce larger agglomerates (Figure S4), and interestingly, the zeta potential becomes negative and small in magnitude, which corresponds to the relatively low stability of the colloid (Figure S5). Therefore, based on the observations described above, we can apply the "balance sheet" approach[39] to the NP migration for 40 nM NP concentration in the situations without electrolyte and with 1 mM TBAP, using the data in Table 1 and with the calculations of transference numbers, t_j,:

$$t_j = \frac{|z_j| C_j u_j}{\sum_i |z_i| C_i u_i} \qquad (11)$$

Where u_j is the mobility of the charged species, and all other symbols have their usual meaning. We note that this approach has been applied to metal NPs before; [25] and we take the basis set of a single ZnO agglomerate of ca. 52 nm reduction which will require 6×10^6 electrons, shown in Figure 4. For the unsupported case depicted in scheme (a), mass transport limits NP reduction, with the rate of migration being the main contributor to the total flux at potentials more negative than -2.4 V vs. Ag/AgCl. Initially, the migration is limited by trace impurities that can balance the movement of the positive particles towards the UME (cathode). As the electrolysis progresses, charged byproducts aid in the transport and help maintain electroneutrality near the electrode surface. This is consistent with our experimental observation that the reduction current tends to increase at longer electrolysis times (Figure 1a), since we find larger spikes and current steps at long experimental times.

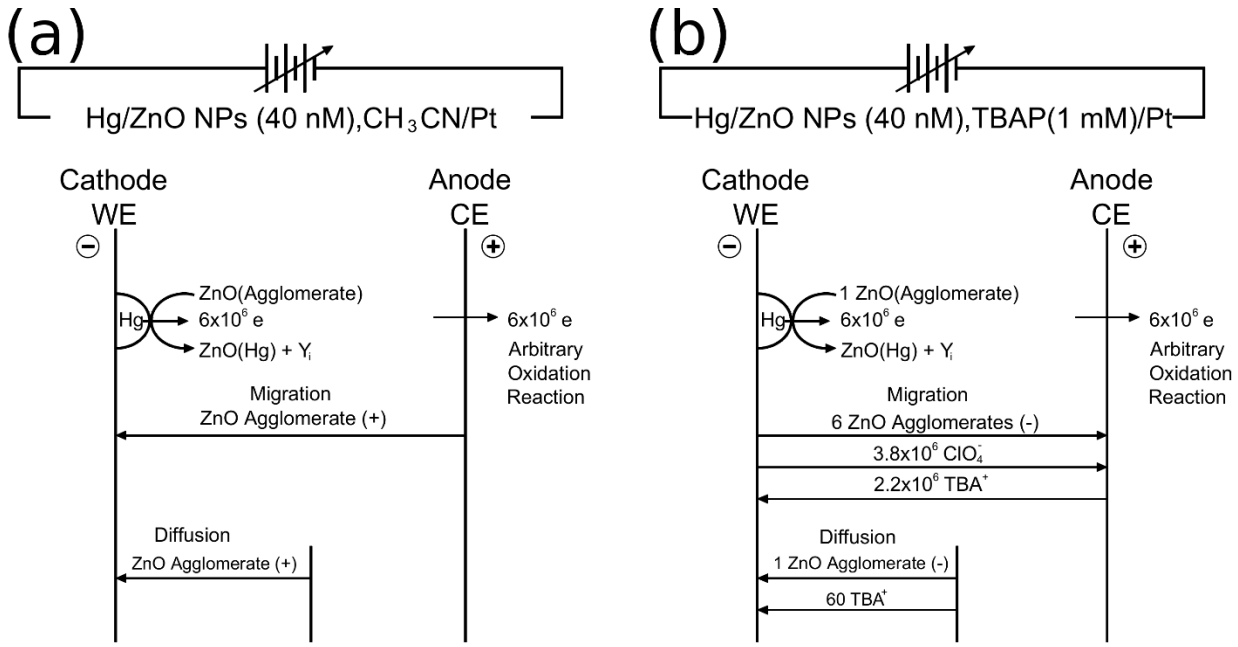

Figure 4. Balance sheets for ZnO NPs colloids (a) unsupported and (b)supported 1 mM TBAP.

The addition of electrolyte increases the size of agglomerates and reverses their charge, as evident on the change on zeta potential sign (Figure S5). We explain the change to a negative zeta potential by the preferential adsorption of ClO_4^- at the NP surface that modifies the original charge at ZnO interface. Figure 4b shows the balance sheet for this case that is unfavorable for the reduction of a negatively charged ZnO agglomerate. The positive charge causes the agglomerate to migrate away from the working electrode and therefore, the NPs must diffuse back to the electrode. A −2 mV zeta potential is not consistent with a stable colloid for the weakly supported colloid, on the other hand, for the unsupported colloid we observed + 13 mV of zeta potential, which is consistent with colloidal stability. The results of the supported case, which has a lower negative −2 mV zeta potential give a nonlinear calibration curve that decreases the stripping charge at higher ZnO concentration. This is consistent with the lower stability of the colloid that increases the agglomerate concentration with higher ZnO concentration. The higher agglomerate concentration, in turn, gives a lower collision frequency that results from the lower diffusion coefficient of the agglomerates. The DLS data, including mobility measurements, and the concentration dependence of the stripping of Zn(Hg) from the ZnO NPs This also explains why the amount of NPs electrolyzed is larger in the unsupported case (Figure 3a) and adding electrolyte decreases the charge (Figure 3b). AlsoIn addition, the stability of the colloid isf a function of the absolute value of the zeta potential; thus, agglomerates are likely to precipitate in this weakly supported colloid.

High-resolution current transients. We measured current transients to study the details of the collisions in terms of the nano-impact electrolysis model.[22] To avoid complications from supporting electrolyte adsorption discussed above, we performed high-resolution experiments in unsupported suspensions. Figure 5 shows the high-resolution data of a single element response for two independent experiments; for (a), the sampling rate was 5 kHz and for (b), the sampling rate was 781 Hz. These higher sampling frequencies allowed us to detect these single entity reduction events. At low sampling frequencies, such as the ones used in Figure 1, we cannot detect these faster events because the reduction decays to the baseline within 100 ms. Note that

the noise in the system at 30 Hz (lower panels of Figure 5a and 5b) cannot be removed using conventional low-pass filters because it is necessary to sample at a higher frequency rate, > 100 Hz. According to the theory, there should be a rapid increase of current followed by a quadratic decay of the current to the baseline.[22] The experimental peaks show a relatively slow increase in current, which to the best of our knowledge, current models cannot adequately describe, although several reports point out that NPs can collide with an electrode surface multiple times, and these could be convoluted into the rising part of the peak due to instrumental limitations (discussed in detail below).[24, 40] Because the total reduction charge is consistent with an agglomerate of it is also possible that during the initial time of the aggregate or agglomerate could bounce off the Hg surface before making contact or that the agglomerate itself reorganizes before reaching a kinetically limited reduction rate. The details of these interactions will be the object of future investigation. Additionally, after the current reaches its maximum, the decay fits the quadratic eq (10) well, with $R^2 > 0.99$. Figure 5a) and b) show the quadratic fitting of two high-resolution collisions to the expanded quadratic model from equation 12:

$$i = \left(\frac{nF\pi}{V_m}\right)\left\{k_f[r_0]^2 - \frac{(k_f)^2}{4} r_0\, t + \frac{(k_f)^3}{16}[t]^2\right\} \qquad (12)$$

Interestingly, the coefficient in the quadratic term in eq. (12), depends on the kinetic constant, k_f, and, the molar volume or crystallographic density, V_m, which is available from crystallographic tables, for ZnO, V_m = 11.805 cm^3/mol [41]. The time-independent term and the linear term in eq. (12), give the radius of the entity and we present these values in Table 3 for three independently measured collisions. In summary, we determine k_f from the quadratic term and we use the other terms to check for consistency (r_o in Table 3). Using a quadratic fit to the experimental data yields values a coefficient with an experimental error of 10%. The error propagation of the fitting error estimates the error in the rate constant, s_{kf}, as discussed in the SI (section S8). Table 3 shows the results of k_f obtained for the two peaks in Figure 5 and one additional peak (data not shown); the values of and s_{kf} indicate the precision of the rate constant measurement.

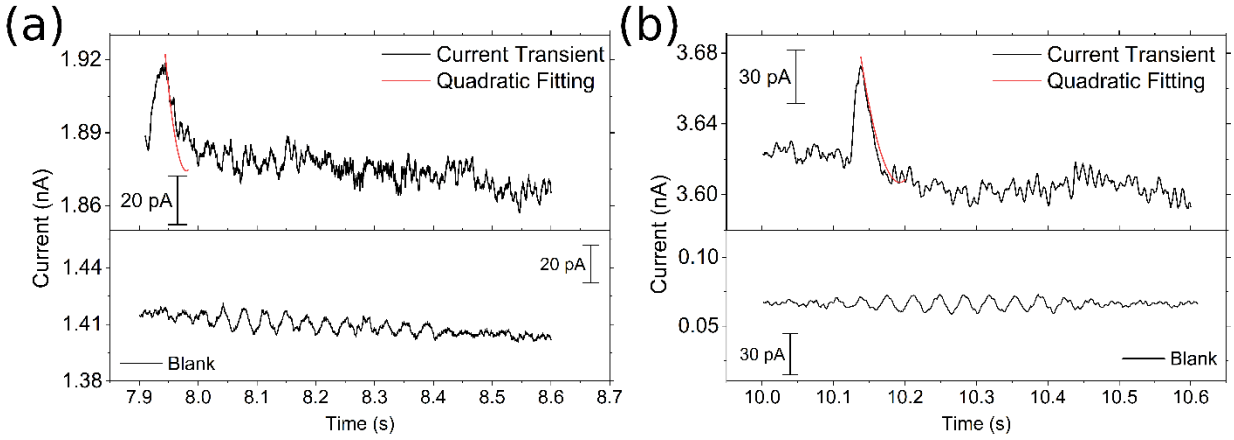

Figure 5. ZnO NPs electrolysis spike in high resolution transients.

Integration of the spike gives the electrolysis charge, Q_I and assuming a perfect sphere being electrolyzed, we solved for r_Q. Overall, the integration is consistent with the reduction transient being due to agglomerates. One of the possible reasons is the sensitivity of the potentiostat used for these measurements because the amount of charge for a single NP reduction would be 6.95 $\times 10^{-15}$ C. If the NP was reduced within 1 ms (the fastest we measured), the reduction current

would be in the order of 10^{-16} A, smaller than our current limit of picoamperes. However, the integrated charge of the transients, r_Q measured from Q_I, is in good agreement with the electrolysis model r_0. The charges measured are consistent with the charge for an agglomerate of 52 nm diameter from DLS, which is expected in the order of 9.8×10^{-13} C. In turn, these results are consistent with the mass transport studies described above and provide additional confidence on the validity of the model used here.

Table 3. Electrolysis spike parameters at high-resolution transients. For a single ZnO NP, the expected charge is 6.96×10^{-15} C.

Trial	Sample Interval, ms	Q_I, C	$r_{Q,}$ [a] nm	r_0, nm	k_f cm/s[b]
1 (Fig 5a)	0.20	8.55×10^{-13}	24.85	17.53	$[2.4 \pm 0.1]\times10^{-4}$
2 (Fig 5b)	1.28	1.25×10^{-12}	28.17	40.63	$[1.7 \pm 0.1]\times10^{-4}$
3 (not shown)	5.12	1.21×10^{-12}	27.87	23.48	$[2.1 \pm 0.1]\times10^{-4}$

a) Calculated with the electrolysis charge
b) Error estimated from the error propagation of the fitting.

Instrumentation effects. Because the time scale of the reduction is within 100 ms, we discuss the instrumentation response time and its effect on the shape of the decay[22-23, 42] and present a method to compensate for the instrumentation effect when determining the rate constant. We measured the time constant of our data acquisition by using a 10 MΩ resistor and the same sampling, sensitivity (1 nA/V) and filtering conditions (150 kHz) as in the collision experiments. We applied a potential step to the resistor and we fitted the response to the step function (more details in ref [7b]):

$$s(t) = k[1 - \exp(-f_o t)] \qquad (13)$$

s(t) is the normalized repose to the step function, and k and f_0 depend on the overall gain of the potentiostat. From fitting to the experimental data, f_0 = 352 Hz, which is the potentiostat cutoff frequency modeled with a low-pass RC filter, where $\tau = 1/f_0 = RC$. The value for the time constant of the potentiostat control is $\tau \approx 3$ ms, and we investigated the effect of instrumentation on reduction events that are in the timescale of < 100 ms. Note that f_0 = 352 Hz for the potentiostat amplification, corresponding to the rise time, is much smaller than the active analog filter of the potentiostat (a Bessel filter with $f_{0,b}$ = 150 kHz), so we consider that the response is limited by the potentiostat rise time. Kanokkanchana et al.[23b] proposed that for accurate peak height measurement, the filtering time constant should be at least 5 – 10 times smaller than the pulse width. The ZnO reduction process here is in the order of 100 ms, and the 3 ms time constant of the potentiostat is within the recommended limits (10 – 20 ms).[23b] Overall, the potentiostat is fast

enough to measure accurately the peak height but we need to discuss the filtering effect of the potentiostat time constant on the shape of the decay. We modeled the effect using a digital approach based on the Fourier transform of an RC filter, $Y(\omega)$, similar to a previously reported,[42] with the same time intervals of the data. Figure 6 shows the analysis of the fast reduction peak in Figure 5a, where Y(t) is the output of the simulated RC filter with τ = 2.84 ms. Figure 6a shows the data and the fit to a model that includes the filter effect, Y(t). For comparison, Figure 6b shows the theoretical response, assuming no filtering effects, and the result of filtering with f_0 = 357 Hz that accounts for the rise time of the potentiostat; as expected the filtering effect is more pronounced at lower times, but the shape of the decay still follows the quadratic decay. A regression of the model including the filter fits the quadratic equation (R^2 = 0.9981) but yields k_f that is significantly different from the raw data fit. Fitting the experimental data we obtained $k_f = (2.4 \pm 0.1) \times 10^{-4}$ cm/s, while considering the filtering contributions, $k_f = (1.8 \pm 0.1) \times 10^{-4}$ cm/s, consistent with the expectation that the filtering effect of the potentiostat yields an apparently slower rate constant.[23a] The error bars from the error propagation of the fit to the raw data, where σ = 10% for the quadratic term. This correction of k_f is consistent with the expectation that the relatively slow potentiostat response results in an smaller value of k_f. The inset in Figure 6a shows the analysis of $k_f = 2 \times 10^{-4}$ cm/s within 5σ for the fitting, that is $k_f = 1 \times 10^{-4}$, 2×10^{-4} and 3×10^{-4} cm/s, to illustrate the sensitivity of the fitting to a model including the filtering effect. These k_f values fit the experimental results in Figure 6a, although the extreme values will fit better the initial or final parts of the decay. Therefore, we propose $k_f = (2 \pm 1) \times 10^{-4}$ cm/s for the reduction of ZnO under these conditions (E = –2.6 V vs NHE in CH_3CN).

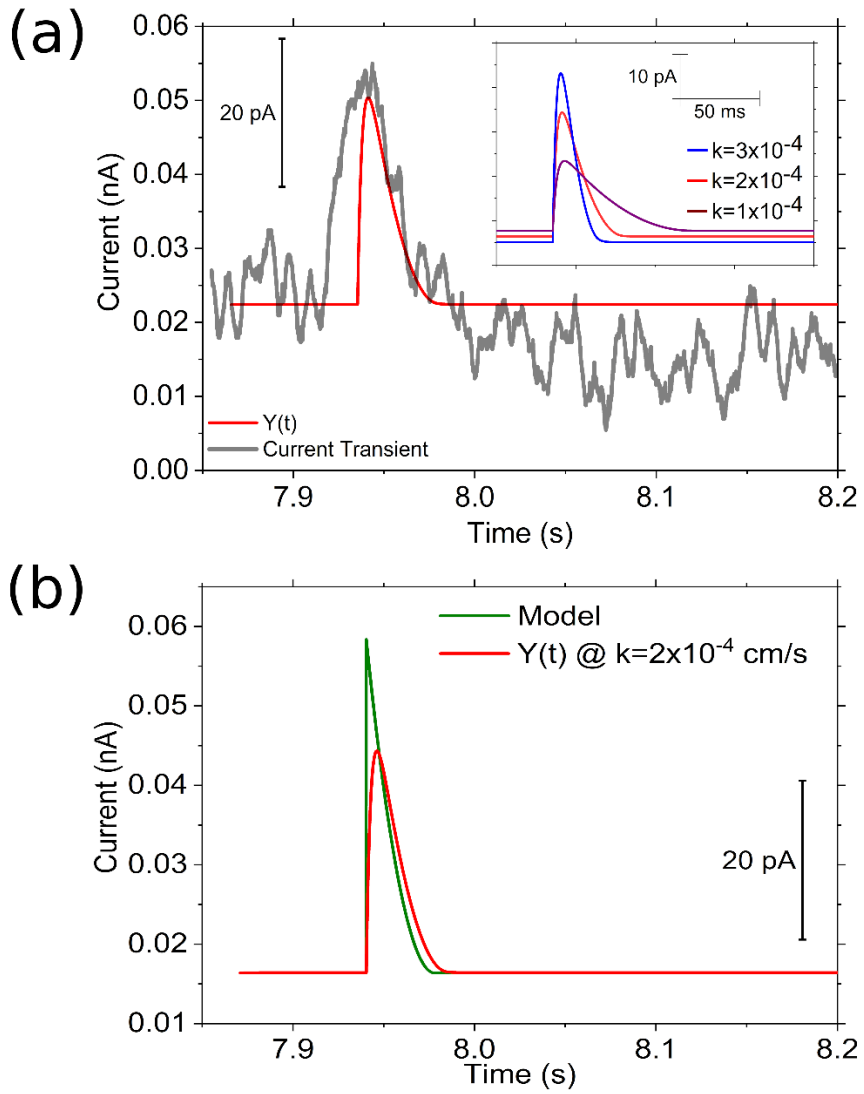

Figure 6. Electrolysis current transient in Figure 5a, with the effect of instrumentation delay simulated as an RC low pass filter, Y(t). (a) electrolysis data (——, black) and model for $k_f = 2 \times 10^{-4}$ including the filtering effect (——, red). The inset shows the results for $k_f = 2 \times 10^{-4} \pm 5\sigma$. (b) Comparison of the model in eq (10) without filtering effects (——, green) and the effect of the RC low-pass filtering, Y(t) on the quadratic model (——, red). All filtering was done with $\tau = RC = 2.84$ s

4. Conclusion

We demonstrate that the models for ionic migration and diffusion are satisfactory in predicting the mass transport of ZnO NPs and their agglomerates when the agglomerate size is constant over the concentration range studied. This explains why the electrochemical reduction of ZnO nanoparticles (NPs) on a Hg UME becomes more sensitive under conditions that favor the migration contribution. Although diffusion is an important contributor to the overall transport, controlling migration has the largest effect on NPs detection. Initially, migration to the UME is

limited because in the absence of supporting electrolyte, trace impurities in the solvent limit the migration of NPs. As the ZnO NP electrolysis progresses, the byproducts introduce ionic species, increasing the migration rate and in turn, making ZnO detection more favorable. Overall, lower detection limits for the experiments performed in the absence of supporting electrolyte are achieved when compared to weakly supported solutions. Addition of supporting electrolyte,1 mM TBAP, has the effect of reversing the agglomerate charge and causing migration away from the working electrode. The diffusion coefficient also decreases because larger aggregates are formed at higher concentration and these effects combine to give a calibration curve with a negative and variable slope. For unsupported systems, we investigated the details of single entities collisions at high sampling rates to resolve the current transient for the reduction of a single agglomerate. The decay fits the quadratic dependence of the model of Kätelhön et al. for the destructive electrolysis nano-impacts. [22] The transients indicate that the reduction of a single agglomerate happens within 100 ms, which is close to the limit of the potentiostat rise time with the trans-impedance needed for current measurements in the order of picoampers. The analysis of the spike yielded the kinetic constant for the electrolysis process of ZnO entities. However, to determine the rate constant at these relatively fast rates, we had to take into account the instrumentation effects. The potentiostat was modeled with as an RC circuit to simulate the reduction data for ZnO agglomerates on a Hg UME, and we propose the rate constant for the process is $k_f = (2 \pm 1) \times 10^{-4}$ cm/s. Overall, the model for destructive electrolysis yields agglomerate sizes that are consistent with the mass-transport analysis and with the sizes obtained from the TEM and DLS measurements. The rate constant obtained for ZnO reduction is significantly smaller than the Ag oxidation constant (ca. 5 cm/s) from stochastic measurements,[24] and from bulk Ag measurements (ca. 0.3 cm/s).[24, 43] This large difference in electron transfer kinetic constants could be because the reduction of Zn^{2+} in ZnO would be a two-electron process limited by the rate-determining step in the reduction mechanism that includes chemical steps. For example, it is possible that the mechanism will be EC or ECE, however, further studies are necessary to account for the significant rearrangement of the Zn^{2+} environment from the solid-state to the Zn(Hg) amalgam, and study the mechanism in detail. For example, it is of interest to our group to investigate the electron transport through the agglomerate and its effect on the reduction kinetics, and these issues will be object of future investigation.

Acknowledgments.
We thank the National Science Foundation (NSF, USA) for support through NSF CHE-1255387 Career award for MAA. Some electrodes were checked using an SEM funded with NSF Grant MRI-1726897. Some of the results were included in Nelum Karunathilake's Ph.D. dissertation.

References

[1] B. M. Quinn, P. G. van't Hof, S. G. Lemay, *J. Am. Chem. Soc.* **2004**, *126*, 8360-8361.

[2] (a) X. Xiao, A. J. Bard, *J. Am. Chem. Soc.* **2007**, *129*, 9610-9612; (b) X. Y. Xiao, F. R. F. Fan, J. P. Zhou, A. J. Bard, *J. Am. Chem. Soc.* **2008**, *130*, 16669-16677.

[3] M. A. Edwards, D. A. Robinson, H. Ren, C. G. Cheyne, C. S. Tan, H. S. White, *Faraday Discuss.* **2018**, *210*, 9-28.

[4] (a) Y. G. Zhou, N. V. Rees, R. G. Compton, *Chem. Phys. Lett.* **2011**, *511*, 183-186; (b) Y. G. Zhou, N. V. Rees, R. G. Compton, *ChemPhysChem* **2011**, *12*, 2085-2087; (c) Y.-G. Zhou, N. V. Rees, R. G. Compton, *Angew. Chem. Int. Ed.* **2011**, *50*, 4219-4221.

[5] N. P. Sardesai, D. Andreescu, S. Andreescu, *J. Am. Chem. Soc.* **2013**, *135*, 16770-16773.
[6] A. Fernando, S. Parajuli, M. A. Alpuche-Aviles, *J. Am. Chem. Soc.* **2013**, *135*, 10894-10897.
[7] (a) K. K. Barakoti, S. Parajuli, P. Chhetri, G. R. Rana, R. Kazemi, R. Malkiewich, M. A. Alpuche-Aviles, *Faraday Discuss.* **2016**, *193*, 313-325; (b) A. Fernando, P. Chhetri, K. K. Barakoti, S. Parajuli, R. Kazemi, M. A. Alpuche-Aviles, *J. Electrochem. Soc.* **2016**, *163*, H3025-H3031.
[8] (a) H. Ma, W. Ma, J. F. Chen, X. Y. Liu, Y. Y. Peng, Z. Y. Yang, H. Tian, Y. T. Long, *J. Am. Chem. Soc.* **2018**, *140*, 5272-5279; (b) Y.-Y. Peng, H. Ma, W. Ma, Y.-T. Long, H. Tian, *Angew. Chem.* **2018**, *130*, 3820-3824; (c) Y.-Y. Peng, H. Ma, W. Ma, Y.-T. Long, H. Tian, *Angew. Chem. Int. Ed.* **2018**, *57*, 3758-3762; (d) R. Gao, Y.-L. Ying, Y.-J. Li, Y.-X. Hu, R.-J. Yu, Y. Lin, Y.-T. Long, *Angew. Chem. Int. Ed.* **2018**, *57*, 1011-1015.
[9] (a) P. Chhetri, K. K. Barakoti, M. A. Alpuche-Aviles, *J. Phys. Chem. C* **2015**, *119*, 1506-1516; (b) N. Perera, N. Karunathilake, P. Chhetri, M. A. Alpuche-Aviles, *Anal. Chem.* **2015**, *87*, 777-784.
[10] J. Zhang, Q. Zhou, Y. Tang, L. Zhang, Y. Li, *Chem. Sci.* **2019**, *10*, 8924-8929.
[11] C. G. Fink, J. D. Prince, *Trans. Am. Electrochem. Soc.* **1929**, *54*, 315.
[12] G. V. Gur'yanov, *Tr. Kuban. S-kh. Inst.* **1974**, *32*, 79-95.
[13] (a) W. W. Dunn, Y. Aikawa, A. J. Bard, *J. Am. Chem. Soc.* **1981**, *103*, 3456-3459; (b) W. W. Dunn, Y. Aikawa, A. J. Bard, *J. Electrochem. Soc.* **1981**, *128*, 222-224.
[14] P. V. Kamat, *J. Chem. Soc., Faraday Trans. 1 F* **1985**, *81*, 509-518.
[15] (a) M. Gratzel, in *Electrochemistry in colloids and dispersions* (Eds.: R. A. Mackay, J. Texter), VCH, New York, **1992**, pp. 357-374; (b) U. Kolle, J. Moser, M. Gratzel, *Inorg. Chem.* **1985**, *24*, 2253-2258.
[16] M. Heyrovsky, J. Jirkovsky, B. R. Mueller, *Langmuir* **1995**, *11*, 4293-4299.
[17] M. Heyrovsky, J. Jirkovsky, M. Struplova-Bartackova, *Langmuir* **1995**, *11*, 4300-4308.
[18] M. Heyrovsky, J. Jirkovsky, M. Struplova-Bartackova, *Langmuir* **1995**, *11*, 4309-4312.
[19] (a) E. Dubois, J. Chevalet, *Langmuir* **2003**, *19*, 10892-10900; (b) I. T. Lucas, E. Dubois, J. Chevalet, S. Durand-Vidal, *Phys. Chem. Chem. Phys.* **2008**, *10*, 3263-3273; (c) I. T. Lucas, E. Dubois, J. Chevalet, S. Durand-Vidal, S. Joiret, *Phys. Chem. Chem. Phys.* **2008**, *10*, 3274-3286.
[20] P. Singh, K. L. Parent, D. A. Buttry, *J. Am. Chem. Soc.* **2012**, *134*, 5610-5617.
[21] E. Fahrenkrug, J. Gu, S. Jeon, P. A. Veneman, R. S. Goldman, S. Maldonado, *Nano Lett.* **2014**, *14*, 847-852.
[22] E. Kätelhön, E. E. Tanner, C. Batchelor-McAuley, R. G. Compton, *Electrochim. Acta* **2016**, *199*, 297-304.
[23] (a) D. O. Wipf, E. W. Kristensen, M. R. Deakin, R. M. Wightman, *Anal. Chem.* **1988**, *60*, 306-310; (b) K. Kanokkanchana, E. N. Saw, K. Tschulik, *ChemElectroChem* **2018**, *5*, 3000-3005.
[24] D. A. Robinson, Y. Liu, M. A. Edwards, N. J. Vitti, S. M. Oja, B. Zhang, H. S. White, *J. Am. Chem. Soc.* **2017**, *139*, 16923-16931.
[25] J. H. Park, A. Boika, H. S. Park, H. C. Lee, A. J. Bard, *J. Phys. Chem. C* **2013**, *117*, 6651-6657.
[26] (a) A. Boika, A. J. Bard, *Anal. Chem.* **2015**, *87*, 4341-4346; (b) J. Bonezzi, A. Boika, *Electrochim. Acta* **2017**, *236*, 252-259; (c) V. Brasiliense, A. N. Patel, A. Martinez-Marrades, J. Shi, Y. Chen, C. Combellas, G. Tessier, F. Kanoufi, *J. Am. Chem. Soc.* **2016**, *138*, 3478-3483; (d) W. Cheng, R. G. Compton, *TrAC, Trends Anal. Chem.* **2014**, *58*, 79-89; (e) S. E. Fosdick, M. J. Anderson, E. G. Nettleton, R. M. Crooks, *J. Am. Chem. Soc.* **2013**, *135*, 5994-5997; (f) Z. T. Gossage, N. B. Schorr, K. Hernandez-Burgos, J. Hui, B. H. Simpson, E. C. Montoto, J. Rodriguez-Lopez, *Langmuir* **2017**, *33*, 9455-9463; (g) K. McKelvey, M. A. Edwards, H. S. White, *J. Phys. Chem. Lett.* **2016**, *7*, 3920-3924; (h) B. H. Meekins, *Phys. Chem. Chem. Phys.* **2017**, *19*, 17256-17262; (i) C. A. Ortiz-Ledon, C. G. Zoski, *Anal. Chem.* **2017**, *89*, 6424-6431; (j) J. J. Yoo, M. J. Anderson, T. M. Alligrant, R. M. Crooks, *Anal. Chem.* **2014**, *86*, 4302-4307; (k) Y. Yu, T. Sun, M. V. Mirkin, *Anal. Chem.* **2015**, *87*, 7446-7453; (l) A. Boika, S. N. Thorgaard, A. J. Bard, *J. Phys. Chem. B* **2013**, *117*, 4371-4380.

[27] (a) K. R. Wehmeyer, R. M. Wightman, *Anal. Chem.* **1985**, *57*, 1989-1993; (b) R. M. Wightman, D. O. Wipf, in *Electroanal. Chem., Vol. 15* (Ed.: A. J. Bard), **1989**, pp. 267-353.
[28] J. C. Myland, K. B. Oldham, *J. Electroanal. Chem.* **1993**, *347*, 49-91.
[29] C. Amatore, B. Fosset, J. Bartelt, M. R. Deakin, R. M. Wightman, *J. Electroanal. Chem.* **1988**, *256*, 255-268.
[30] K. B. Oldham, *J. Electroanal. Chem.* **1992**, *337*, 91-126.
[31] J. J. Watkins, H. S. White, *Langmuir* **2004**, *20*, 5474-5483.
[32] E. Kätelhön, R. G. Compton, *ChemElectroChem* **2015**, *2*, 64-67.
[33] H.-Q. Shi, W.-N. Li, L.-W. Sun, Y. Liu, H.-M. Xiao, S.-Y. Fu, *Chem. Commun.* **2011**, *47*, 11921-11923.
[34] N. Karunathilake, Gutierrez-Portocarrero, M. A. Alpuche-Aviles, *manuscript in preparation* **2019**.
[35] S. J. Kwon, H. Zhou, F.-R. F. Fan, V. Vorobyev, B. Zhang, A. J. Bard, *Phys. Chem. Chem. Phys.* **2011**, *13*, 5394-5402.
[36] (a) R. Dasari, K. Tai, D. A. Robinson, K. J. Stevenson, *ACS Nano* **2014**, *8*, 4539-4546; (b) R. Dasari, B. Walther, D. A. Robinson, K. J. Stevenson, *Langmuir* **2013**, *29*, 15100-15106.
[37] R. J. Hunter, in *Foundation of colloid science*, 2nd ed., Oxford, UK, **2001**, pp. 33-40.
[38] J. Barthel, L. Iberl, J. Rossmaier, H. J. Gores, B. Kaukal, *J. Solution Chem.* **1990**, *19*, 321-337.
[39] A. J. Bard, L. R. Faulkner, *Electrochemical methods: fundamentals and applications*, 2nd ed., John Wiley & Sons, New York, **2001**.
[40] (a) S. M. Oja, D. A. Robinson, N. J. Vitti, M. A. Edwards, Y. Liu, H. S. White, B. Zhang, *J. Am. Chem. Soc.* **2017**, *139*, 708-718; (b) J. Ustarroz, M. Kang, E. Bullions, P. R. Unwin, *Chem. Sci.* **2017**, *8*, 1841-1853; (c) W. Ma, H. Ma, J.-F. Chen, Y.-Y. Peng, Z.-Y. Yang, H.-F. Wang, Y.-L. Ying, H. Tian, Y.-T. Long, *Chem. Sci.* **2017**, *8*, 1854-1861.
[41] P. K. Davies, A. Navrotsky, *J. Solid State Chem.* **1981**, *38*, 264-276.
[42] D. A. Robinson, M. A. Edwards, H. Ren, H. S. White, *ChemElectroChem* **2018**, *5*, 3059-3067.
[43] (a) H. Gerischer, *Z. Elektrochem.* **1958**, *62*, 256; (b) H. Gerischer, R. P. Tischer, *Z. Elektrochem.* **1957**, *61*, 1159; (c) D. Larkin, N. Hackerman, *J. Electrochem. Soc.* **1977**, *124*, 360.